Structure, Dynamics, and Power Conversion Efficiency Correlations in a New Low Bandgap Polymer: PCBM Solar Cell

Jianchang Guo,[†,‡] Yongye Liang,[‡] Jodi Szarko,[§] Byeongdu Lee,[∥] Hae Jung Son,[‡] Brian S. Rolczynski,[§] Luping Yu,*[,‡] and Lin X. Chen*[,†,§]

Chemical Science and Engineering Division, Argonne National Laboratory, 9700 South Cass Avenue, Argonne, Illinois 60439, Department of Chemistry and James Franck Institute, The University of Chicago, 929 East 57th Street, Chicago, Illinois 60637, Department of Chemistry, Northwestern University, 2145 Sheridan Road, Evanston, Illinois 60208, and X-ray Science Division, Advanced Photon Source, Argonne National Laboratory, Argonne, Illinois 60439

Received: September 22, 2009; Revised Manuscript Received: December 7, 2009

Molecular packing structures and photoinduced charge separation dynamics have been investigated in a recently developed bulk heterojunction (BHJ) organic photovoltaic (OPV) material based on poly(thienothiophene-benzodithiophene) (PTB1) with a power conversion efficiency (PCE) of >5% in solar cell devices. Grazing incidence X-ray scattering (GIXS) measurements of the PTB1:PCBM ([6,6]-phenyl-C_{61}-butyric acid methyl ester) films revealed π-stacked polymer backbone planes oriented parallel to the substrate surface, in contrast to the π-stacked polymer backbone planes oriented perpendicular to the substrate surface in regioregular P3HT [poly(3-hexylthiophene)]:PCBM films. A ~1.7 times higher charge mobility in the PTB1:PCBM film relative to that in P3HT:PCBM films is attributed to this difference in stacking orientation. The photoinduced charge separation (CS) rate in the pristine PTB1:PCBM film is more than twice as fast as that in the annealed P3HT:PCBM film. The combination of a small optical gap, fast CS rate, and high carrier mobility in the PTB1:PCBM film contributes to its relatively high PCE in the solar cells. Contrary to P3HT:PCBM solar cells, annealing PTB1:PCBM films reduced the device PCE from 5.24% in the pristine film to 1.92% due to reduced interfacial area between the electron donor and the acceptor. Consequently, quantum yields of exciton generation and charge separation in the annealed film are significantly reduced compared to those in the pristine film.

Introduction

Since their discovery about 15 years ago, bulk heterojunction (BHJ) organic photovoltaic (OPV) devices made from semiconducting polymers have shown promise for future commercialization due to their low cost, ease of fabrication, and small environmental impact relative to silicon and heavy metal based semiconductor solar cells.[1−3] To achieve a high power conversion efficiency (PCE) in solar cells based on BHJ OPV materials, the semiconducting polymer composites must be efficient in light harvesting, exciton splitting, charge carrier generation, and transport.[4,5] Additionally, the effective charge carrier collection must be optimized by minimizing the carrier trapping at the interfaces between the photoactive organic materials and the electrodes. These processes in the current OPV devices are far from ideal. Several challenges need to be addressed, such as raising the PCE and improving the long-term photochemical stability, before practical applications of OPV can be realized.[2,6−8]

One of the main reasons for the low PCE in OPV devices is the limited overlap of their absorption spectra with the solar spectrum. For example, one of the most studied semiconducting polymers, poly-3-hexylthiophene (P3HT), only harvests photons with wavelengths <650 nm. Therefore, organic materials with lower optical transition energies are attractive materials for photovoltaics because they can harvest solar photons with long wavelengths, particularly in the near-infrared (NIR) region.[8−13] Recently, we reported a new series of low bandgap polymers with alternating ester-substituted thieno[3,4-b]thiophene and dialkoxyl benzodithiophene units, PTB1 (Figure 1, inset).[10] Prototype devices prepared from the pristine blend of this polymer and [6,6]-phenyl-C-butyric acid methyl ester (PCBM) exhibit >5% PCE. Compared to the state-of-the-art P3HT:PCBM devices, the PTB1:PCBM device has a photocurrent ~30% higher and a similarly high fill factor of >65% with little sacrifice of the open circuit voltage, V_{oc}. We have recently achieved a PCE of 6.1% in solar cells based on the BHJ composites involving a modular change of the side groups presented in PTB1.[14]

To understand why these polymers have such favorable characteristics, we have investigated correlations of the structure, dynamics, and efficiency of the PTB1:PCBM system. Grazing incidence X-ray scattering (GIXS) was used to identify film structural characteristics on different length scales (e.g., molecular packing, degree of crystallinity, and statistically averaged morphologies).[15,16] Meanwhile, ultrafast transient absorption (TA) spectroscopy was used to probe the dynamics of fundamental processes in OPV materials, such as exciton generation, charge separation (CS), and charge recombination (CR). The GIXS studies identified a unique lamellar packing structure in

* Corresponding authors. Lin X. Chen. Phone: (630)252-3533. Fax: (630)252-9289. E-mail: lchen@anl.gov or l-chen@northwestern.edu. Luping Yu. Phone: (773)702-8698. Fax: (773)702-0805. E-mail: lupingyu@ychicago.edu.
[†] Chemical Science and Engineering Division, Argonne National Laboratory.
[‡] The University of Chicago.
[§] Northwestern University.
[∥] X-ray Science Division, Advanced Photon Source, Argonne National Laboratory.

10.1021/jp909135k
Published on Web 12/28/2009

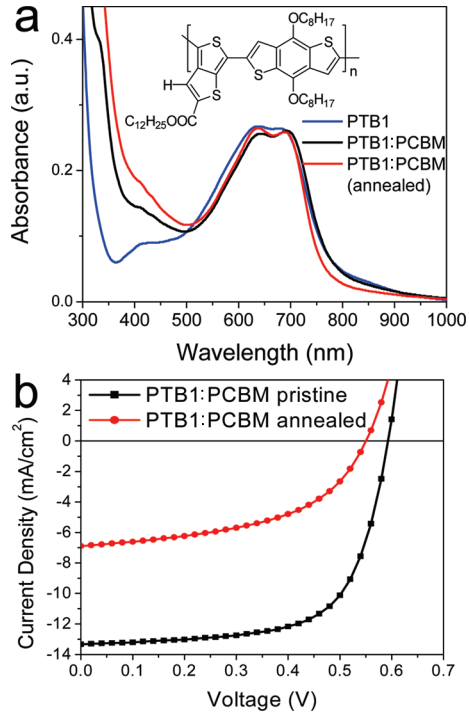

Figure 1. (a) Normalized UV−vis spectra of PTB1, PTB1:PCBM at 1:1 (weight ratio), and annealed 1:1 films. The inset is the molecular structure of PTB1 polymer. (b) Current−voltage characteristic solar cell devices (ITO/PDOT-PSS/PTB1:PCBM/Ca/Al) made by PTB1:PCBM 1:1 pristine and annealed films under the AM 1.5 condition (100 mW/cm^2).

the PTB1:PCBM films with both the π-conjugated backbone and the side chains *parallel* to the substrate. This unique molecular packing is the main reason behind the higher carrier mobility observed in the devices based on PTB1 devices than in P3HT devices. The TA studies revealed that the CS rate in the PTB1:PCBM film is more than twice as fast as that of the P3HT:PCBM film. The enhanced absorptive overlap with the solar spectrum, faster CS rate, and higher carrier mobility all contribute to the high PCE of the PTB1:PCBM devices.

Experimental Section

Film/Substrate Preparation and Device Fabrication. The polymer, PTB1, was synthesized according to a previously reported method.[10] Silicon substrates with PEDOT:PSS (Baytron P VP A1 4083) were used for samples in GIXS measurements. Glass substrates were used for samples in ultrafast optical measurements. For the standard device fabrication, PTB1 and PCBM were codissolved in 1,2-dichlorobenzene (DCB) in a 1:1 weight ratio. The ITO-coated glass substrate was cleaned stepwise in detergent, water, acetone, and isopropyl alcohol under ultrasonication for 10−30 min each and subsequently dried in an oven for 5 h. A thin layer (∼30 nm) of PEDOT:PSS (Baytron P VP A1 4083) was spin-coated onto the ITO surface, which was pretreated by ultraviolet ozone for 15 min. After being baked at 120 °C for ∼20 min, the substrates were transferred into a nitrogen-filled glovebox (<0.1 ppm of O_2 and H_2O). A ca. 100 nm thick PTB1:PCBM composite layer was then spin-cast from the blended solution at 800−1000 rpm on the ITO/PEDOT:PSS substrate without further treatment. Subsequently, the film was transferred to a thermal evaporator located in the same glovebox. Furthermore, a 25 nm Ca layer and 80 nm Al layer were deposited in sequence under the vacuum of 2×10^{-6} Torr. The effective area was measured to be 0.095 cm^2. The current density vs voltage ($J-V$) curves were measured using a Keithley 2400 source measure unit. The photocurrent was measured under AM 1.5 G illumination at 100 mW/cm^2 under a Newport Thermal Oriel 91192 1000 W solar simulator (4″ × 4″ beam size). The light intensity was determined by a monosilicon detector (with KG-5 visible color filter) calibrated by the National Renewable Energy Laboratory (NREL) to reduce spectral mismatch.

Femtosecond Transient Absorption Spectroscopy. Ultrafast transient absorption (TA) spectroscopic measurements in the visible region were carried out using a Spectra Physics laser system consisting of a Mai-Tai Ti:sapphire oscillator coupled with a Spitfire Pro XP regenerative amplifier operated at 1 kHz repetition rate and a home-built optical parametric amplifier (OPA) that was described previously.[17] The pulse width (fwhm) from the Spitfire is about 100 fs with a pulse energy of 3 mJ/pulse. The excitation laser pulses were derived from the output of the OPA at 600 nm. The white light continuum probe pulses were generated by focusing a few microjoules of the Ti:sapphire amplifier output onto a sapphire disk. The resulting white light beam was split into the reference and the probe beams. The white light probe beam and the pump beam were focused to a 0.3 mm diameter spot at the sample with a nearly collinear geometry. The laser is capable of achieving a maximum 300 nJ (∼100 nJ with OPA output) pulse energy, but the pulse energy used in our measurements was determined by the pulse energy dependence of the kinetics as described in the Results section. The instrumental response function was 180 fs at fwhm.

Ultrafast TA spectra and kinetics in the near-infrared (NIR) region were carried out at the Center for Nanoscale Materials at Argonne National Laboratory using a Ti:Sapphire laser system from Spectra Physics and a data acquisition system from Ultrafast Systems, Inc.[9] The laser system consists of an oscillator, a regenerative amplifier, and an optical parametric amplifier (OPA), which was operated at 5 kHz repetition rate. Laser pulses with pulse duration of 100 fs at full width at half-maximum (fwhm) and pulse energy of 10 nJ at 600 nm were obtained. The transient absorption spectrometer enables simultaneous three-dimensional data collection (spectra/kinetics/ΔOD) for probe wavelengths of 450−750 nm and 850−1600 nm. The excitation wavelength was 600 nm for all samples. The optical density of each sample was <0.4 at 600 nm. The instrumental response function was 120−150 fs at fwhm. A CCD detector was used to collect the data in the spectral region of 500−750 nm, while a GaAs detector was used to collect the data in the spectral region of 900−1600 nm.

Grazing Incidence X-ray Scattering (GIXS) Measurements. Grazing incidence wide-angle X-ray scattering (GI-WAXS) measurements were performed using Beamline 12BM of the Advanced Photon Source (APS) at Argonne National Laboratory. Scattering intensities are expressed as a function of the scattering vector, $q = 4\pi/\lambda \sin \theta$, where θ is the half scattering angle and $\lambda = 1.5498$ Å is the wavelength of the incident radiation. The d-spacing of a peak is expressed by $2\pi/q$. The samples were kept under vacuum during irradiation to minimize the radiation damage to the films from the X-ray beam. A two-dimensional area MAR detector was used to collect the scattering images and was situated at 129.3 mm from the sample for GIWAXS measurements. The films were illuminated at an incidence angle of about 0.2° by the X-rays at 8 keV, so that the X-ray beam could penetrate the entire thickness of the film and only a very small portion of the substrate, minimizing the background scattering from the substrate.

Grazing incidence small-angle X-ray scattering (GISAXS) measurements were carried out at Beamline 8ID of the APS, with $\lambda = 1.6868$ Å. Similarly, samples were kept under the vacuum during the measurements, and a MAR detector at 1308.8 mm from the sample was used to collect the scattering images.

Results and Discussion

Light Harvesting Enhancements. Compared to P3HT films, PTB1 films have a red-shifted absorption onset, broadening the spectral overlap with the solar spectrum. Meanwhile, the PTB1 film also has a higher peak absorbance than the P3HT film with an extinction coefficient of 7.5×10^4 cm^{-1} at 690 nm,[14] compared to 6×10^4 cm^{-1} at 550 nm for P3HT films.[18] Consequently, PTB1 films can harvest solar photons more effectively than P3HT films with the same thickness. Figure 1a shows the UV−vis spectra for films of PTB1 and PTB1:PCBM blend (1:1 weight ratio for all the blend films in this report) before and after annealing. A broad peak in the 626−687 nm region is due to the characteristic $\pi-\pi^*$ transition of the PTB1 polymer with a bandgap of ~1.60 eV.[10] After the polymer is blended with PCBM, the absorption feature at 687 nm for the composite film shifts to 695 nm, while a new peak at 333 nm appears due to the absorption of PCBM. Annealing the PTB1:PCBM film at 120 °C for 30 min hardly alters optical properties except for a slightly blue-shifted absorption onset. In contrast, absorption spectra of the P3HT/PCBM films were significantly red-shifted after the annealing, which was attributed to flattened polymer backbones with longer conjugation lengths in more ordered structure.[19] The difference in spectral responses after the annealing suggests that the backbone of PTB1 may be rather rigid without annealing because (a) the thienothiophene moiety is known for inducing a rigid quinoidal structure of the backbone and (b) the benzodithiophene moiety with three fused aromatic rings is a completely rigid entity. Therefore, the annealing process does not increase the backbone rigidity.

***I*−*V* Characteristics.** Figure 1b shows the *I*−*V* curves for the solar cells made of both pristine and annealed PTB1:PCBM films (ITO/PEDOT-PSS/PTB1:PCBM/Ca/Al). The devices were illuminated under AM 1.5 conditions with a power density of 100 mW/cm^2. The device made from pristine film has an open circuit voltage (V_{oc}) of 0.6 V, a short circuit current (J_{sc}) of 13.3 mA/cm^2, and a fill factor (FF) of 65.8%, corresponding to a PCE of 5.24%. The device made from an annealed film has $V_{oc} = 0.56$ V, $J_{sc} = 6.9$ mA/cm^2, FF = 49.6%, and a PCE of 1.92%, much lower than the pristine film device, which is in contrast to the findings of more conventional polymers such as P3HT.[20]

Morphology Characteristics. To optimize solar cell efficiencies, bicontinuous electron donor and acceptor channels with large interfacial interactions between them are essential for effective exciton splitting, charge separation, and charge transport.[2] Therefore, morphological control of the photoactive layer is crucial to maximize the device performance. TEM images of pristine and annealed PTB1:PCBM films (1:1, w/w) are displayed in Figure 2. The former has fine intertwined fibrous features (i.e., ~5 nm width), suggesting a better donor−acceptor interaction,[10] whereas the latter shows large phase-separated PCBM-enriched domains (10−200 nm in size), suggesting reduced domain interfacial boundaries between PTB1 and PCBM and thereby a lower exciton splitting efficiency. This morphological change in the film is also related to the observed charge separation dynamics to be described later.

Molecular Packing Structures in Films. Since exciton splitting and charge separation in BHJ OPV devices take place at the molecular level, knowing the molecular packing structural origins related to the high PCE in PTB1:PCBM films is important for optimizing the devices. To acquire structural details, GISAXS and GIWAXS techniques were used to probe molecular packing orientation relative to the substrate surface and intermolecular *d*-spacing in the neat PTB1 and PTB1:PCBM blend films. The molecular packing structures in films are revealed by the GISAXS (Figure 3a,b) and GIWAXS (Figure 3c,d) images of pristine PTB1 and PTB1:PCBM (1:1 w/w) films. In a simplified model, the diffraction features distributed in the vertical or *z*-axis of the image give the lattice spacing out of the film plane, and those in the horizontal or the *y*-axis give the lattice spacing in the film plane. The PTB1 film presents a feature in horizontal or *y*-axis at $q_y = 0.23$ Å^{-1} ($d_a = 27.3$ Å) (Figure 3a and Figure 3f inset) and a distinctive feature in vertical or *z*-axis at $q_z = 1.71$ Å^{-1} ($d_b = 3.7$ Å) (Figure 3c). The latter ($d_b = 3.7$ Å) is a typical π-stacking spacing of polymer backbones (Figure 3e), and its paralleled appearance in the vertical direction indicates that these polymer backbones are parallel to the film plane. With this picture in mind, the former ($d_a = 27.3$ Å) is most likely due to the interstack spacing in the film plane (Figure 3e) in the absence of PCBM. These results suggest that PTB1 molecules are assembled and oriented with the π-conjugated backbones stacked parallel to the substrate surface and with the interstack separation of 27.3 Å defined by the side chains extended outward from the backbone parallel to the substrate (Figure 3e).

In comparison, the scattering images of the PTB1:PCBM (1:1) composite film (Figures 3b, d) as well as the scattering profile along the *y*-axis (Figure 3f, inset) show the peak corresponding to the interstack spacing at $q_y = 0.24$ Å^{-1} ($d_a = 26.2$ Å), while the scattering peak along the *z*-axis corresponding to the π-stacked polymer backbone spacing stays unchanged in the *q*-value but with a reduced intensity that suggests reduced π-stacking order possibly due to the intercalation of PCBM between the polymer chains (Figure 3f). An intense, nearly spherically distributed scattering feature near $q \approx 0$ (Figure 3b) is attributed to either PCBM domains or the fibrous morphological features with 5 nm or larger in size observed by TEM (Figure 2). Additional broad rings in the scattering pattern from the PTB1:PCBM film (Figure 3d) at $q_{y,z} = 1.41$ Å^{-1} ($d = 4.46$ Å) and $q_{y,z} = 0.73$ Å^{-1} ($d = 8.6$ Å) coincide with the *q*-values for (311) and (111) Bragg diffractions in neat C_{60} samples.[21,22] The spherical symmetry of these scattering features manifests random PCBM domain orientations with respect to the substrate surface. In both PTB1 and PTB1:PCBM films, PTB1 retains a lamellar structure with the polymer backbone planes and side chains parallel to the surface. The GIWAXS profiles along the *z*-axis (Figure 3f) show that the PTB1 π-stacking and PCBM peak intensities increase after the annealing due to the growth in the

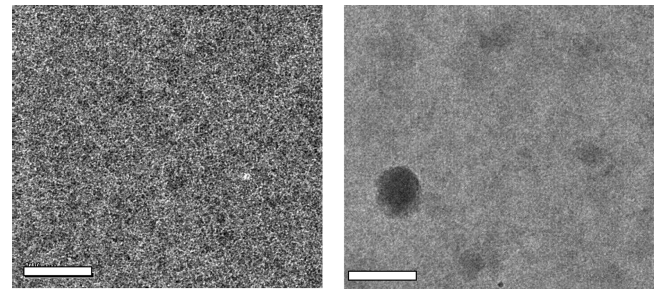

Figure 2. TEM of a pristine film of PTB1:PCBM (1:1) (left) and an annealed film of PTB1:PCBM (1:1) (right). Large PCBM domains were only observed in the annealed film. The dimension of the scale bar in the images is 200 nm.

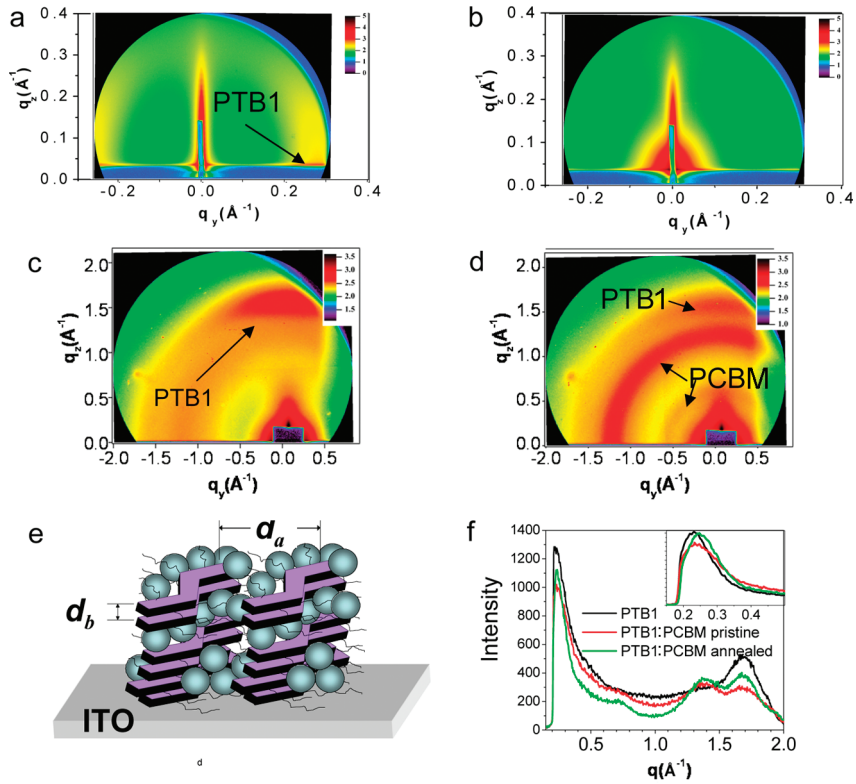

Figure 3. GISAXS images of (a) polymer PTB1 and (b) pristine PTB1:PCBM (1:1) film. GIWAXS images of (c) polymer PTB1 and (d) pristine PTB1:PCBM (1:1) film. (e) Schematic illustration of the orientation of the PTB1 polymer with polymer backbone and side chain parallel to the substrate. The interstack and $\pi-\pi$ stacking distances are labeled as d_a and d_b, respectively. (f) Out-of-plane linecuts of GIWAXS. The inset shows the expanded view of in-plane linecuts for $q = 0.15-0.5$ Å^{-1}, which are collected at a different MARS CCD camera position.

crystallinity for PTB1 and PCBM domains, while the π-stacking orientation of PTB1 remains unchanged.

Sizes of PTB1 π-stacked domains can be estimated from the Scherrer equation[23]

$$D_{hkl} = \frac{0.9\lambda}{\beta_{hkl}\cos\theta} \quad (1)$$

where D_{hkl} is the dimension of the diffracting lattice domain along [*hkl*] direction; β_{hkl} is the full width at half-maximum of the [*hkl*] diffraction peak (in radians); and θ is the angular position of the peak. Because the π-stacking peaks of PTB1 partially overlap with the intramolecular scattering signals of PCBM, the width of each peak, β_{hkl}, can only be extracted by curve-fitting the peaks in the region of $q = 1-2$ Å^{-1} to two Gaussian functions. The average size of the PTB1 π-stacking domains is estimated to be 25 Å, corresponding to approximately seven π-stacked polymer chains.

Dynamics of Exciton Splitting, Charge Separation, and Charge Recombination. It has been well-recognized that the OPV function in BHJ solar cells has multistep processes of exciton splitting, charge separation, carrier generation, and diffusion[24] involving singlet/triplet excitons (ES), localized charge transfer state (CT), polymer cations, and PCBM anions. The transitions from one species to another can be correlated in space, time, and energy. Transient absorption (TA) spectroscopy was used to characterize each of these multistep processes individually in a time window of ~100 fs to a few nanoseconds. From this information, we could shed light on structure-dynamics correlations in OPV functions. Within this time window, the TA spectra of the PTB1:PCBM film after the excitation could contain contributions from various species

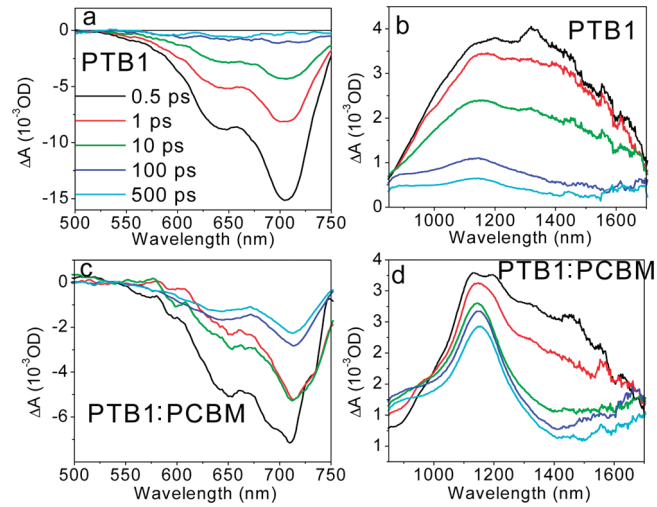

Figure 4. TA spectra of pristine PTB1 film in the visible region (a) and the NIR region (b) and the pristine PTB1:PCBM (1:1) film in the visible (c) and NIR region (d) with the 600 nm light excitation.

mentioned above. TA spectra of PTB1 and PTB1:PCBM films in the visible region (Figure 4a,c) and the NIR region (Figure 4b,d) were measured. The PTB1 film exhibited a negative ground state bleaching feature at 706 nm with a shoulder feature at 642 nm and a positive broad singlet exciton absorption peak centered around 1350 nm. The exciton feature vanished almost completely at 500 ps after the excitation. In addition, a new peak at 1150 nm started to emerge at 100 ps after the excitation and was sustained with the same shape at 500 ps delay. This peak was assigned to the PTB1 cation absorption,[25] similar to those observed in other conjugated polymers,[26,27] and was confirmed by the absorption spectra of the same film undergoing

an electrochemical oxidation. Although the binding energy of the exciton in conducting polymers is considerably higher than kT at room temperature, the dissociation of excitons into ionic species or the production of low yield photocurrent has been observed and attributed to the asymmetry of the films imposed by the work functions of two different electrodes or the surface effect.[28] Therefore, observing cation species in neat polymer is not surprising because the measurements have been conducted with thin films with about 100 nm thickness.

The TA spectra in the PTB1:PCBM composite film (Figure 4d) are very different from those of the neat films, where the initial broad exciton absorption quickly transformed into a distinct peak at 1150 nm with a shoulder feature at 1320 nm within 0.5 ps of the excitation. Noticeably, the 1150 nm peak differed in shape from the broad exciton absorption band and grew as the exciton absorption decayed. As verified above, this 1150 nm peak was due to the cation formation with a lifetime much longer than a few nanoseconds in the composite film. Another emerging absorption was also observed in the near-infrared (NIR) region above 1500 nm, which is assigned to the second cation absorption as confirmed by the absorption spectra of the PTB1:PCBM film undergoing an electrochemical oxidation. Similar cation absorption features in the infrared region were also reported in photoinduced absorption spectra of regioregular and regiorandom P3HT.[29] Because of the spectral limit in the TA measurements, the exact position of the second absorption band for the cation is unclear but is estimated near 1930 nm from the curve fitting. This NIR peak and the first cation absorption peak at 1150 nm are well separated. Therefore, we used the intensity of the 1150 nm peak to characterize the cation yield as shown below.

Effect of Annealing on the Charge Separation Dynamics. It has been recorded from previous studies that the annealing of P3HT:PCBM films enhanced the PCE in solar cells due to an increased ordering in P3HT domains characterized by red-shifted optical absorption features.[19,30] Conversely, the annealing of a PTB1:PCBM film reduced the device PCE by a factor of 2.7 to 1.92% from 5.24% prior to annealing. To reveal the reasons behind the different PCE responses after the annealing of the films, we compared the TA signals of PTB1 cations in the pristine and annealed films at 1150 nm as a function of the probe delay time (Figure 5a). The intensities of the dynamics signals at 1150 nm were normalized by the number of photons absorbed at the pump wavelength of 600 nm, while the cation yields of the films were characterized by the signal level at 2.5 ns after the excitation. The TA signal intensity at 1150 nm at this delay time for the annealed film was only about 43% of that for the pristine film. Such a reduction was a result of the reduced interfacial area between donor and acceptor after annealing as evidenced from TEM images (Figure 2b). Consequently, the device with the annealed PTB1:PCBM film had a substantially lower PCE than that with the pristine film.

Pathways from Exciton to Charge Separated State. According to our TA results in the NIR spectral region (Figure 4b,d), the singlet exciton absorption was so broad that it overlapped with the PTB1 cation absorption, causing difficulties in identifying contributions from different species immediately after the photoexcitation. To extract individual contributions from all possible species in the TA spectra from which the CS and CR dynamics are obtained, a quantitative model of the population dynamics was established by fitting the TA spectra of the PTB1:PCBM film as a sum of absorptions from a singlet exciton, free PTB1 cation, and PCBM anion, as expressed by eq 2.

$$S(\lambda, t) = N_{ES}(t)A_{ES}(\lambda) + N_{CS}(t)[A_c(\lambda) + A_a(\lambda)] + N_{CT}(t)A_{CT}(\lambda) \quad (2)$$

where $S(\lambda,t)$ was the signal in the NIR window at the detection wavelength λ and at delay time t; $N_{ES}(t)$, $N_{CS}(t)$, and $N_{CT}(t)$ were populations of singlet PTB1 exciton, charge separated PTB1 cation, or PCBM anion, and charge transfer intermediate, $PTB1^{+}PCBM^{-}$, respectively; and they were varied in the fitting. $A_c(\lambda)$ was the absorption spectrum of the cation, obtained from the TA spectrum of the PTB1:PCBM composite film at 515 ps delay time, in which two Gaussian functions centered at 1143 and 1930 nm were used, respectively. The latter peak with a lower energy corresponded to the free carrier absorption. $A_{ES}(\lambda)$ was the absorption spectrum of the single exciton, obtained from the TA spectrum of the neat PTB1 film at 0.2 ps delay time, was also fit by two Gaussian functions with peak positions at 1111 and 1446 nm, respectively. $A_a(\lambda)$ was the anion spectrum, also obtained from the TA spectrum of the PTB1:PCBM film at 515 ps delay time by fitting the high energy part of the spectrum using two Gaussian functions with peak positions at 1154 and 873 nm, respectively. $A_{CT}(\lambda)$ was the unknown spectrum for the charge transfer intermediate. We initially looked for any detectable residual contribution after taking the difference between the experimental spectrum $A_{EXP}(\lambda)$ and the summed TA spectrum with only contributions from the singlet excitons and the cations or anions, $A_{SUM}(\lambda) = \{N_{ES}(t)A_{ES}(\lambda) + N_{CS}(t)[A_c(\lambda) + A_a(\lambda)]\}$. The contribution from $A_{CT}(\lambda)$ was

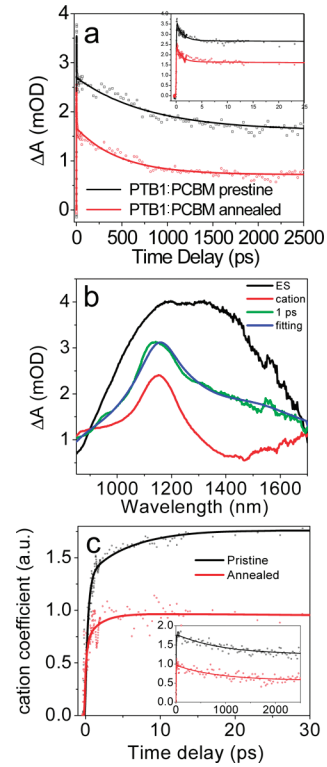

Figure 5. (a) Kinetic traces of pristine and annealed films monitored at 1150 nm, normalized by the number of photons absorbed at 600 nm. The inset shows the same kinetic traces at early delay time. (b) An example of spectral fitting at 1 ps delay time for the PTB1:PCBM films by using eq 2. The spectrum of a singlet exciton (labeled as ES) is obtained from a 0.2 ps spectrum of neat PTB1 film, and the cation spectrum is obtained from the spectrum of PTB1:PCBM at 515 ps. (c) Fitting coefficient of the PTB1 cation at different time delay for the pristine and annealed films by using eq 2. The inset shows the same kinetic traces at longer delay time.

expected to appear if the residuals from the subtraction of $A_{EXP}(\lambda)$ from $A_{SUM}(\lambda)$ were statistically significant. However, that was not the case. Instead, $A_{EXP}(\lambda)$ and $A_{SUM}(\lambda)$ overlapped very well with each other within the experimental error (Figure 5b). Therefore, only the singlet excitons and the cations or anions had statistically significant contributions in this spectral region. Although the spectra shown here could not identify any charge transfer intermediate state, $PTB1^{+}PCBM^{-}$ with bound ion pairs, it could not be ruled out entirely because (a) its optical signatures could be outside of the spectral window in our experiments and (b) its lifetime was too short and hence its transient concentration was too low to detect. We plan to collect the TA spectra in the 750−850 nm region and to detect emissive species by fluorescence upconversion in the NIR region in the future to probe possible intermediate CT states in this system.

The experimental TA spectra of the PTB1:PCBM composite films are decomposed into PTB1 cation and PCBM anion[31,32] absorptions as shown in the support information. (Figure S1, Supporting Information) The population decay and growth kinetics of the charge-separated species, cations, and anions, (Figure 5c) extracted from fitting the experimental TA spectra for the pristine and annealed PTB1:PCBM films, could be expressed by biexponential rise and biexponential decay functions. The biexponential rise of the cation formation kinetics suggested two possible pathways for the cation formation. For the pristine film, the rise time constants were 0.37 ps (76%) and 5.9 ps (24%), and the decay time constants were 931 ps (30%) and >2.5 ns (70%). For the annealed film, the rise time constants were 0.27 ps (62%) and 2.0 ps (38%), and the decay time constants were 836 ps (41%) and >2.5 ns (59%). Compared to the pristine film, the annealed film had a faster CS rate and a comparable CR rate. However, its initial CS state population observed in the transient absorption spectroscopy and in the cation population density (Figure 5c) is significantly lower than those in the pristine film, which explained a much lower PCE for the device made from the annealed film than that from the pristine film.

Structural Factors Affecting the Device PCE. From the GIXS results of P3HT:PCBM composite films, the annealed film exhibited a lamellar structure with the backbone and side chains dominantly normal to the substrate surface.[19,33] The enhanced device PCE after the annealing was attributed to better carrier mobility of the P3HT:PCBM film due to the improved intrachain ordering and interchain stacking.[19] Using the solvent annealing approach, the PCE of the P3HT:PCBM device was enhanced further, attributed to even stronger polymer ordering with the same backbone and side chain orientations.[34] In contrast, the GIXS results of PTB1 films suggested a unique lamellar packing structure with the conjugated backbone planes of alternating thienothiophene-benzodithiophene units and side chains *parallel* to the substrate. From a solar cell application standpoint, such an orientation of the molecular packing structure in PTB1:PCBM films is ideal for electrons or holes to be transported away from their generation point and for charge collection at the material/electrode interface with maximized contact between the polymer backbones with the electrodes. The advantage of this molecular packing is evidenced by 67% higher charge carrier mobility observed in PTB1 films compared to that in P3HT films (4.5×10^{-4} $cm^2/v \cdot s$ for PTB1 and 2.7×10^{-4} $cm^2/v \cdot s$ for P3HT).[10]

The averaged CS rate for pristine PTB1:PCBM film is 1.5 ps, which is 2.7 times of that of 4 ps for the annealed P3HT/PCBM film.[35] This faster CS rate, combined with higher charge carrier mobility resulting from a lamellar structure with side chain parallel to the substrate, may contribute to the high device PCE for the PTB1:PCBM solar cell. The improvement of light absorption in the NIR region can also contribute to the high efficiency. Because of the complexity in the fundamental photophysical processes, directly connecting dynamics to the device performance would be very difficult. However, we are seeking to quantify and separate individually the attributes from the above factors to the improved performance of the PTB1:PCBM device.

The efficiency of the devices with the PTB1:PCBM films dropped more than 50% after the annealing. The GIXS results show that the $\pi-\pi$ stacking is more ordered, while the intermolecular stack spacing decreases slightly. Meanwhile, PCBM domains 10−200 nm in size are formed as observed in the TEM images for the annealed film (Figure 2b). The increased PCBM domain size will decrease the effective interfacial area between PTB1 and PCBM, which will subsequently reduce the charge separation and charge collection efficiencies. As evidenced by the ultrafast transient spectroscopy (Figure 5a), the free charge density decreases by more than a half after the annealing, which is the result of decreased effective interfacial area and becomes a key factor in limiting the efficiency.

Summary

In summary, our studies correlating structure, dynamics, and efficiency in PTB1:PCBM composite films revealed several factors that may contribute to a relatively high PCE of >5% by this new low bandgap polymer. Possible efficiency enhancing factors are: (1) a broad absorption spectrum in the NIR region harvesting more solar photons, (2) a high miscibility between the polymer donor and PCBM acceptor up to molecular level which enhances interfacial interactions resulting in a high exciton splitting efficiency, and (3) a parallel conjugated polymer backbone plane relative to the electrode surface and the effective π-stacking of the polymer backbones result in an efficient charge transport through interchain interactions and a relatively high carrier mobility (66% higher than P3HT). We believe that the results will provide new insights in future designs of new efficient polymer BHJ solar cells.

Acknowledgment. We would like to acknowledge the support by UC/ANL Collaborative Research Seed Grant (L.Y. and L.X.C.), Northwestern University Setup Fund, and the U.S. Department of Energy, Office of Science, Office of Basic Energy Sciences under Contracts DE-AC02-06CH11357 (Argonne National Laboratory) (for L. X. C.). We are thankful for the support from NSF, AFOSR, and NSF MRSEC grant for the University of Chicago (for L.P.Y.). We thank Dr. David J. Gosztola for his help in the transient absorption facility at the Center for Nanoscale Materials of Argonne National Laboratory and Drs. Joseph W. Strzalka and Sonke Seifert of the Advanced Photon Source for their help at the beamline setup and useful discussions in data analysis for GIXS. Work at the Advanced Photon Source and the Center for Nanoscale Materials was supported by the U.S. Department of Energy, Office of Science, Office of Basic Energy Sciences, under Contract No. DE-AC02-06CH11357.

Note Added after Print Publication. This paper was published on the Web on December 28, 2009, and in the January 21, 2010, issue. An author name was misspelled. The electronic version was corrected and reposted to the Web issue on March 11, 2010. An Addition and Correction was also published (DOI: 10.1021/jp102023n).

Supporting Information Available: The details of the curve fitting for Figure 5b and 5c and the fitting parameters are included. This material is available free of charge via the Internet at http://pubs.acs.org.

References and Notes

(1) Yu, G.; Gao, J.; Hummelen, J. C.; Wudl, F.; Heeger, A. J. *Science* **1995**, *270*, 1789.
(2) Thompson, B. C.; Frechet, J. M. J. *Angew. Chem., Int. Ed.* **2008**, *47*, 58.
(3) Li, G.; Shrotriya, V.; Yao, Y.; Huang, J.; Yang, Y. *J. Mater. Chem.* **2007**, *17*, 3126.
(4) Bredas, J.-L.; Beljonne, D.; Coropceanu, V.; Cornil, J. *Chem. Rev.* **2004**, *104*, 4971.
(5) Coropceanu, V.; Cornil, J.; Da Silva Filho, D. A.; Olivier, Y.; Silbey, R.; Bredas, J.-L. *Chem. Rev.* **2007**, *107*, 926.
(6) Park, S. H.; Roy, A.; Beaupre, S.; Cho, S.; Coates, N.; Moon, J. S.; Moses, D.; Leclerc, M.; Lee, K.; Heeger, A. J. *Nat. Photonics* **2009**, *3*, 297.
(7) Campoy-Quiles, M.; Ferenczi, T.; Agostinelli, T.; Etchegoin, P. G.; Kim, Y.; Anthopoulos, T. D.; Stavrinou, P. N.; Bradley, D. D. C.; Nelson, J. *Nat. Mater.* **2008**, *7*, 158.
(8) Lee, J. K.; Ma, W. L.; Brabec, C. J.; Yuen, J.; Moon, J. S.; Kim, J. Y.; Lee, K.; Bazan, G. C.; Heeger, A. J. *J. Am. Chem. Soc.* **2008**, *130*, 3619.
(9) Liang, Y.; Feng, D.; Guo, J.; Szarko, J. M.; Ray, C.; Chen, L. X.; Yu, L. *Macromolecules* **2009**, *42*, 1091.
(10) Liang, Y.; Wu, Y.; Feng, D.; Tsai, S.-T.; Son, H.-J.; Li, G.; Yu, L. *J. Am. Chem. Soc.* **2009**, *131*, 56.
(11) Liang, Y.; Xiao, S.; Feng, D.; Yu, L. *J. Phys. Chem. C* **2008**, *112*, 7866.
(12) Peet, J.; Kim, J. Y.; Coates, N. E.; Ma, W. L.; Moses, D.; Heeger, A. J.; Bazan, G. C. *Nat. Mater.* **2007**, *6*, 497.
(13) Wienk, M. M.; Struijk, M. P.; Janssen, R. A. J. *Chem. Phys. Lett.* **2006**, *422*, 488.
(14) Liang, Y.; Feng, D.; Wu, Y.; Tsai, S.-T.; Li, G.; Ray, C.; Yu, L. *J. Am. Chem. Soc.* **2009**, *131*, 7792.
(15) Chabinyc, M. L. *Polym. Rev.* **2008**, *48*, 463.
(16) Yoon, J.; Choi, S.; Jin, S.; Jin, K. S.; Heo, K.; Ree, M. *J. Appl. Crystallogr.* **2007**, *40*, s669.
(17) Guo, J.; Liang, Y.; Xiao, S.; Szarko, J. M.; Sprung, M.; Mukhopadhyay, M. K.; Wang, J.; Yu, L.; Chen, L. X. *New J. Chem.* **2009**, *33*, 1497.
(18) Cook, S.; Furube, A.; Katoh, R. *Energy Environ. Sci.* **2008**, *1*, 294.
(19) Kim, Y.; Cook, S.; Tuladhar, S. M.; Choulis, S. A.; Nelson, J.; Durrant, J. R.; Bradley, D. D. C.; Giles, M.; McCulloch, I.; Ha, C.-S.; Ree, M. *Nat. Mater.* **2006**, *5*, 197.
(20) Kim, Y.; Choulis, S. A.; Nelson, J.; Bradley, D. D. C.; Cook, S.; Durrant, J. R. *Appl. Phys. Lett.* **2005**, *86*, 063502/1.
(21) Stephens, P. W.; Mihaly, L.; Lee, P. L.; Whetten, R. L.; Huang, S. M.; Kaner, R.; Deiderich, F.; Holczer, K. *Nature* **1991**, *351*, 632.
(22) Woo, C. H.; Thompson, B. C.; Kim, B. J.; Toney, M. F.; Frechet, J. M. J. *J. Am. Chem. Soc.* **2008**, *130*, 16324.
(23) Chiu, M.-Y.; Jeng, U. S.; Su, C.-H.; Liang, K. S.; Wei, K.-H. *Adv. Mater.* **2008**, *20*, 2573.
(24) Ohkita, H.; Cook, S.; Astuti, Y.; Duffy, W.; Tierney, S.; Zhang, W.; Heeney, M.; McCulloch, I.; Nelson, J.; Bradley, D. D. C.; Durrant, J. R. *J. Am. Chem. Soc.* **2008**, *130*, 3030.
(25) An, Z.; Wu, C. Q.; Sun, X. *Phys. Rev. Lett.* **2004**, *93*, 216407.
(26) Moses, D.; Dogariu, A.; Heeger, A. J. *Phys. Rev. B* **2000**, *61*, 9373.
(27) Sheng, C. X.; Tong, M.; Singh, S.; Vardeny, Z. V. *Phys. Rev. B* **2007**, *75*, 085206.
(28) Marks, R. N.; Halls, J. J. M.; Bradley, D. D. C.; Friend, R. H.; Holmes, A. B. *J. Phys.-Condes. Matter* **1994**, *6*, 1379.
(29) Osterbacka, R.; An, C. P.; Jiang, X. M.; Vardeny, Z. V. *Science* **2000**, *287*, 839.
(30) Li, G.; Shrotriya, V.; Huang, J.; Yao, Y.; Moriarty, T.; Emery, K.; Yang, Y. *Nat. Mater.* **2005**, *4*, 864.
(31) Guldi, D. M.; Hungerbiihler, H.; Janata, E.; Asmus, K.-D. *J. Phys. Chem.* **1993**, *97*, 11258.
(32) Kato, T.; Kodama, T.; Oyama, M.; Okazaki, S.; Shida, T.; Nakagawa, T.; Matsui, Y.; Suzuki, S.; Shiromaru, H.; Yamauchi, K.; Achiba, Y. *Chem. Phys. Lett.* **1991**, *186*, 35.
(33) Sirringhaus, H.; Brown, P. J.; Friend, R. H.; Nielsen, M. M.; Bechgaard, K.; Langeveld-Voss, B. M. W.; Spiering, A. J. H.; Janssen, R. A. J.; Meijer, E. W.; Herwig, P.; De Leeuw, D. M. *Nature (London)* **1999**, *401*, 685.
(34) Li, G.; Yao, Y.; Yang, H.; Shrotriya, V.; Yang, G.; Yang, Y. *Adv. Funct. Mater.* **2007**, *17*, 1636.
(35) Hwang, I.-W.; Moses, D.; Heeger, A. J. *J. Phys. Chem. C* **2008**, *112*, 4350.

JP909135K